AJNR

Abnormal Magnetization Transfer Ratios in Normal-appearing White Matter on Conventional MR Images of Patients with Occlusive Cerebrovascular Disease

Hirotsugu Kado, Hirohiko Kimura, Tatsuro Tsuchida, Yoshiharu Yonekura, Tomoo Tokime, Yasuhiko Tokuriki and Harumi Itoh

AJNR Am J Neuroradiol 2001, 22 (5) 922-927
http://www.ajnr.org/content/22/5/922

AJNR Am J Neuroradiol 22:922–927, May 2001

Abnormal Magnetization Transfer Ratios in Normal-appearing White Matter on Conventional MR Images of Patients with Occlusive Cerebrovascular Disease

Hirotsugu Kado, Hirohiko Kimura, Tatsuro Tsuchida, Yoshiharu Yonekura, Tomoo Tokime, Yasuhiko Tokuriki, and Harumi Itoh

BACKGROUND AND PURPOSE: **Chronic hypoperfusion may cause ischemic insult in the deep white matter. The magnetization transfer phenomenon is associated with the amount and constitution of myelin. The purpose of this study was to assess the usefulness of the magnetization transfer ratio (MTR) for detecting vasculometabolic abnormalities on positron emission tomography (PET) studies in patients with unilateral severe stenosis of the internal carotid artery (ICA).**

METHODS: **MTR maps and PET data—including regional cerebral blood flow (rCBF), regional cerebral metabolic rate of oxygen ($rCMRO_2$), and regional oxygen extraction fraction (rOEF)—were investigated in 13 patients with unilateral severe stenosis of the ICA. The same regions of interest were selected in the white matter both on MTR maps and PET scans. The areas were classified into three groups based on MTR values (group 0, MTR >47.22%; group 1, MTR = 45.77% to 47.22%; group 2, MTR <45.77%), and the relationship between MTR and PET data was analyzed by means of both absolute values and asymmetric index (AI).**

RESULTS: **Abnormal values could not be detected in the areas classified as group 0. The areas classified as group 1 were characterized by absolutely normal values of $rCMRO_2$ and increased rOEF with AI, which was assessed as viable and reversible on the PET study. The areas classified as group 2 showed decreased $rCMRO_2$ with absolute values, which was considered irreversible in PET. A significant overall linear correlation was found between MTR and $rCMRO_2$ values.**

CONCLUSION: **Using the MTR technique to classify ischemic damage into three groups (normal, reversible, and irreversible), we found a significant correlation between the reduction of MTR and that of $rCMRO_2$ in white matter with ICA stenosis. We believe that the MTR technique may partly replace PET data in the assessment of ischemic injury.**

The magnetization transfer (MT) technique has been used as a means of changing image contrast. MT is related to relaxation properties associated with immobile protons of neighboring macromolecules in tissue membranes and bulk free water. An off-resonance radio-frequency pulse is applied to saturate immobile protons. Any exchange of this saturated pool of protons with the protons in the surrounding bulk free water will change the signal intensity seen on subsequent MR images (1–5). In brain tissue, the cholesterol-containing lipid bilayer of myelin is regarded as the major macromolecule responsible for the MT phenomenon (6). Once the constitutional changes of the macromolecule in myelin occur, the exchanges between bound and bulk free water protons might occur less frequently than in normal brain tissue, thus causing the reduction of magnetization transfer ratios (MTRs). Therefore, the MTRs are thought to reflect changes in the amount and constitution of myelin present in white matter. The measurement of MTRs has proved to be useful for characterizing some types of brain disease, such as multiple sclerosis (7, 8), wallerian degeneration (9), and diffuse axonal injury (10).

In chronic internal carotid artery (ICA) occlusion, long-standing hypoperfusion may cause ischemic insult in the deep white matter, often resulting in infarction (11, 12). Even in noninfarcted white matter regions, metabolic changes have been detected and assessed both by positron emission to-

Received July 13, 2000; accepted after revision November 15.

From the Department of Radiology (H.Ka., H.ki., T.Tsu., H.I.) and Biomedical Imaging Research Center (Y.Yo.), Fukui Medical University, Fukui; and Department of Neurosurgery (T.To., Y.To.), Fukui Red Cross Hospital, Fukui, Japan

Address reprint requests to Hirotsugu Kado, MD, Department of Radiology, Fukui Medical University, 23 Shimoaizuki, Matsuoka, Yoshida-gun, Fukui 910–1193, Japan.

TABLE 1: Demographic and clinical data for 13 patient with unilateral severe stenosis of the internal carotid artery (ICA)

Patient No.	Age (y)/Sex	ICA Stenosis (Right/Left)	Percentage of Stenosis (%)
1	56/M	R	99
2	60/F	R	75
3	65/F	R	75
4	68/M	R	90
5	66/M	R	80
6	64/M	R	95
7	74/F	L	90
8	84/M	L	90
9	75/M	R	90
10	72/F	R	80
11	54/M	L	99
12	63/M	L	90
13	55/M	R	80

mography (PET) and proton MR spectroscopy (13, 14). The sensitivity of MTR measurement is superior to that of conventional MR images in detecting abnormalities in white matter in some diseases (7, 8). Therefore, we hypothesized that abnormal MTRs would be closely related to the compromised metabolic state in noninfarcted white matter with severe stenosis of the ICA.

In the current study, we measured MTRs and correlated them with vasculometabolic parameters obtained by PET in patients with chronic occlusive cerebrovascular disease. Our goal was to evaluate the usefulness of the MTR technique for detecting vasculometabolic abnormalities in PET data in patients with unilateral severe stenosis of the ICA.

Methods

Subjects

Thirteen patients with unilateral severe stenosis of the ICA participated in this study. Ages ranged from 54 to 84 years old, with a mean age of 65.8 ± 8.8 years. The patients were selected on the basis of the following criteria: 1) no cortical infarction other than minimal subcortical abnormality as revealed by MR images, and angiographic evidence of more than 75% stenosis in caliber or occlusion of the common carotid artery; and 2) collateral vessel circulation through the anterior portion of the circle of Willis (cross-flow) in the presence of unilateral severe stenosis of the ICA. The demographic and clinical data for all subjects are summarized in Table 1. All subjects gave written informed consent to a protocol approved by the committee for clinical research of this institute.

MR Measurement

Conventional MR images were obtained in all subjects on a 1.5-T scanner. Anatomic MR images were obtained with a T1-weighted sagittal spin-echo sequence using parameters of 350/14 (TR/TE). Fast spin-echo (FSE) T2-weighted images were acquired before calculation of the MTR maps. Parameters for the T2-weighted images were 3500/84, a section thickness of 5 mm with a 2-mm gap, a field of view (FOV) of 22 cm, and an acquisition matrix of 256 × 192.

Using the gradient-recalled acquisition in the steady state (GRASS) technique with (M_s) and without (M_0) an MT saturation pulse, MTR maps were calculated on a pixel-by-pixel basis using the following equation:

$$MTR = (M_0 - M_s) / M_0 \times 100\ (\%).$$

Parameters for the GRASS sequence were 600/4, a flip angle of 20 °, a section thickness of 5 mm with a 2-mm gap, an FOV of 22 cm, and an acquisition matrix of 256 × 128. Magnetization transfer (M_s) was performed with a single sinc-shaped pulse irradiating 1.5 kHz off-resonance from water. The duration and peak were 17 milliseconds and 1.4 times higher than that of the 90° pulse, respectively. Although the pulses were used in every 50 milliseconds under 12 multislice TR = 600 acquisition, the power deposition was well within the limitation of the signal absorption rate. The patient's head was carefully positioned for the comparison with PET scans. The acquired tomographic slices were parallel to the orbitomeatal line on the MR images.

PET Measurement

Within 3 hours after the MR study, cerebral blood flow (CBF), cerebral metabolic rate of oxygen ($CMRO_2$), and oxygen extraction fraction (OEF) were measured using a PET scanner equipped with an 18-ring detector arrangement. The physical characteristics of this PET scanner have been described in detail by DeGrado et al (15). With axial continuous gantry motion, this scanner provides 35 transaxial images simultaneously with an interval space of 4.25 mm. Axial and transaxial resolutions were 4.2 mm, allowing multidirectional reconstruction of the images without loss of resolution. The spatial resolution of the reconstructed PET scans was 6 mm in full width at half-maximum intensity (FWHM) at the center of the FOV. The FOV and pixel size of the reconstructed images were 256 and 2 mm, respectively. The patient's head was carefully positioned such that the midsagittal plane of the head was parallel to the camera's sagittal plane using a laser-beam pointer for comparison with the MR images. A 10-minute transmission scan was acquired with a 68-Ge/68-Ga source for attenuation correction.

The steady-state method and [^{15}O]-labeled CO_2 were used for regional CBF (rCBF) measurements. After patients continuously inhaled [^{15}O]-labeled CO_2, their PET data continued to be recorded under the steady-state condition for 10 minutes. Three arterial blood samples were obtained from the radial artery, and their radioactivity concentrations were counted using a well counter cross-calibrated to the PET scanner. After the rCBF study, regional OEF (rOEF) was measured by means of the continuous inhalation of [^{15}O]-labeled O_2 and by the method described by Lammertsma and coworkers (16, 17). Using the rCBF and rOEF values, regional cerebral metabolic rate of oxygen ($rCMRO_2$) was calculated pixel by pixel. The acquired tomographic slices were parallel to the orbitomeatal line on PET studies.

Data Analyses

Region of Interest (ROI) Selection.—CBF, $CMRO_2$, and OEF images obtained by PET were registered with the MR images of each subject by means of statistical parametric mapping using software (from the Welcome Department of Cognitive Neurology, London, UK) implemented in Matlab (Mathworks, Inc, Sherborn, MA).

After registration, we selected seven ROIs on the lesional side in each subject and the same ROIs at the level of the ventricular body both on the MTR maps and the PET scans (CBF, $CMRO_2$, and OEF). The circular, 21-mm-diameter ROIs were the same for both the PET and MR images. To obtain exact values from the PET data, the ROI diameter needed to be more than three times the FWHM of the PET scans (6 mm). The same examinations were performed on MTR maps and PET scans on the contralateral side in each subject (Fig 1).

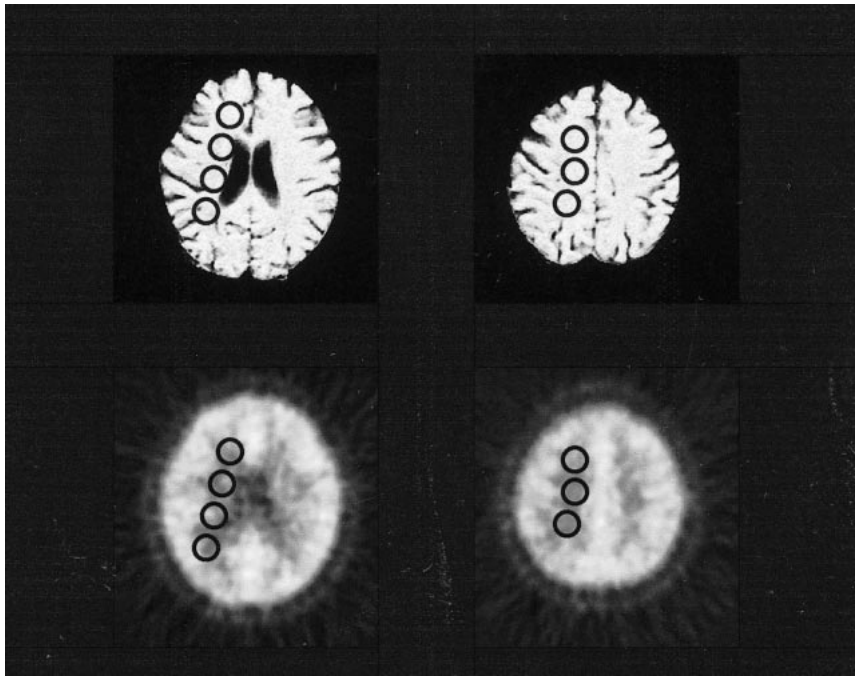

FIG 1. The location of selected ROIs. Four ROIs were selected in the lesional deep white matter and three in the lesional centrum semiovale. Although this figure shows that ROIs were placed only on MTR maps and CBF images, actually the same ROIs were selected on T2-weighted images and other PET scans ($CMRO_2$ and OEF images). PET scans were registered to the MR images of each subject. Circular ROIs were placed in right and left symmetrical locations, so that the AI could be calculated.

TABLE 2: Mean values of absolute regional cerebral blood flow (rCBF), absolute regional cerebral metabolic rate of oxygen ($rCMRO_2$), absolute regional oxygen extraction fraction (rOEF), normalized T2-weighted images, and rOEF asymmetric index (AI) from the lesional side in 13 patients with unilateral severe stenosis of the internal carotid artery by group*

	Absolute rCBF (mL/100 g per min)	Absolute $rCMRO_2$ (mg/100 g per min)	Absolute rOEF	Normalized T2 intensity	rOEF-AI
Group 0	24.43 ± 4.21	2.18 ± 0.12	0.50 ± 0.08	0.45 ± 0.03	1.25 ± 3.22
Group 1	21.06 ± 4.75	2.00 ± 0.23	0.57 ± 0.11	0.47 ± 0.02	13.23 ± 6.06
Group 2	17.72 ± 5.93	1.51 ± 0.29	0.56 ± 0.09	0.58 ± 0.11	12.35 ± 5.17
Infarction	10.13 ± 4.37	0.58 ± 0.37	0.25 ± 0.06	0.85 ± 0.13	−68.48 ± 18.18

* Group 0, MTR > 47.22%; group 1, MTR = 45.77% to 47.22%; group 2, MTR < 45.77%.

Note.—Absolute values of rCBF gradually decreased from group 0 to group 2. Absolute values of $rCMRO_2$ were maintained within the normal range in groups 0 and 1, but those in group 2 decreased significantly ($P = .0003$). Although no definite difference in rOEF between group 0 and 1 were recognized quantitatively, increased rOEF-AI was seen in group 1 ($P = .0003$). The normalized T2-weighted value in group 2 were significantly higher than those in group 1 ($P = .0002$).

Asymmetric Index (AI).—To compare the values of $rCMRO_2$, rOEF, and MTR on the ipsilateral side of severe ICA stenosis, we also measured the values with the same parameters used in the contralateral position and calculated the AI to find latent abnormalities that could not be detected with absolute values.

The AI was calculated in each ROI using the following equation (18):

$$AI = (R_i - R_c) / (R_i + R_c) \times 2 \times 100\ (\%)$$

where R_i and R_c are the ROI values in the ipsilateral and contralateral white matter, respectively.

Normalized Values on T2-Weighted Images.—All values obtained on T2-weighted images were normalized by CSF intensity to compare the same ROIs in all subjects. We located the ROI in the lateral ventricle to obtain the CSF intensity on T2-weighted images.

Group Classification.—To analyze the relationship between MTRs and vasculometabolic rates obtained from PET, we classified ROIs into three groups on the basis of MTR values. Since the average value of MTR obtained from normal white matter on the contralateral side was 50.12 ± 1.45%, we classified the areas with MTR values of more than 47.22% as group 0, those with MTR values from 45.77% to 47.22% as group 1, and those with MTR values of less than 45.77% as group 2. A value of 47.22% was defined as less than −2 SD of normal MTR ranges, and a value of 45.77% was defined as less than −3 SD. Student's *t*-test was performed among the three groups in regard to each parameter obtained from PET. A *P* value of less than .05 was considered significant.

Results

Demographic and clinical information for the 13 subjects are summarized in Table 1, and the locations of selected ROIs are shown in Figure 1.

A total of 91 ROIs were classified into three groups: group 0, 34 areas from nine patients; group 1, 28 areas from seven patients; and group 2, 29 areas from eight patients. The patients were overlapped among the three groups.

Table 2 shows the mean values of quantitative rCBF, quantitative $rCMRO_2$, quantitative rOEF, normalized T2-weighted values, and rOEF obtained by using the AI technique (rOEF-AI) in each group (groups 0, 1, and 2). Absolute values of rCBF grad-

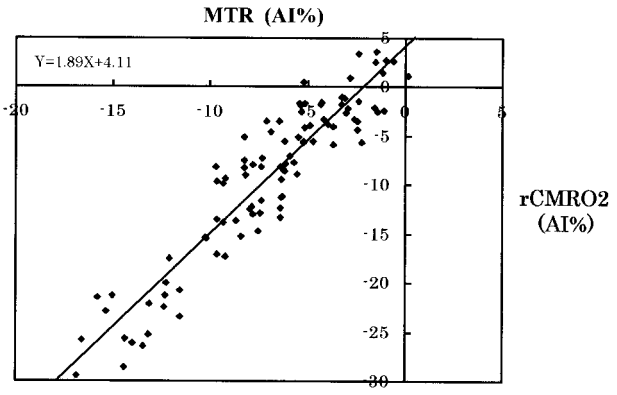

FIG 2. 2D plot of MTR and $rCMRO_2$ values with an AI from groups 0, 1, and 2. The correlation coefficient was .85 ($P = .001$).

ually decreased from group 0 to group 2. Absolute values of $rCMRO_2$ were maintained within the normal range in groups 0 and 1, but those in group 2 decreased significantly ($P = .0003$). Although no significant differences were found in regard to the absolute values of rOEF between groups 0 and 1, the rOEF-AI in group 1 was statistically higher than that in group 0 ($P = .0003$). The normalized T2-weighted values in group 2 were significantly higher than those in group 1 ($P = .0002$).

Figure 2 is a 2D plot of MTR with AI (MTR-AI) and $rCMRO_2$ values with AI ($rCMRO_2$-AI) for all groups. The overall linear correlation between MTR-AI and $rCMRO_2$-AI ($r = .85$; $P = .001$) was significant.

Discussion

The MT effect is induced by applying an off-resonance radio-frequency pulse, as has been demonstrated previously (1–5). The radiation generated by the pulse causes protons bound to macromolecules to become selectively saturated and to exchange spins with free water protons. The exchange of partially saturated spins into the water proton pool decreases the observed magnetization of water protons, leading to hypointensity on the MT image as compared with an equivalent image obtained without radio-frequency saturation pulses. The reduction of intensity on the image with radiation is expressed as decreased MTRs.

In cerebral white matter, the cholesterol-containing lipid bilayer of myelin is postulated to be the major macromolecule responsible for the MT phenomenon (6). The amount of the lipid bilayer is controlled by membrane synthesis and degeneration (19). The balance between membrane synthesis and degeneration is often affected by the condition of the brain tissue; for example, in tissue associated with multiple sclerosis or metabolic disease, or that in an ischemic state (20–24).

According to previous studies using PET (25–31), changes of rCBF, $rCMRO_2$, and rOEF in the brain tissue have been analyzed in relation to cerebral perfusion pressure (CPP). Although autoregulation maintains the constancy of rCBF over a wide range of CPP (25, 26), the rCBF is decreased when CPP has been lowered about 50 mm Hg by decreasing the arterial pressure. Despite the decrease in rCBF when the CPP is reduced by approximately 30 mm Hg, the $rCMRO_2$ is still maintained or slightly decreased (25), because the oxygen demand of the brain tissue is compensated by the increased rOEF. In areas of increased rOEF, autoregulation and CO_2 responsiveness are poor (30), but brain tissue has viability and reversibility. If rCBF is decreased further by the reduction of CPP, the $rCMRO_2$ decreases significantly, because the oxygen demand of the brain tissue cannot be compensated by rOEF. This brain tissue state is considered irreversible (25).

It is important to understand the differences between deep white matter and the cortical region in regard to the nature of blood supply. The deep white matter is supplied mainly by many final microarteriole of lenticulostriate arteries, which are variable and independent of one another and that play separate autoregulatory roles; on the other hand, the cortex is supplied directly by large primary vessels and cortical collaterals. An infarction in deep white matter tends to be spotty, multiple, and heterogeneous, whereas an infarction in the cortex is a large lesion. Therefore, ischemic deep white matter is also considered to be heterogeneous tissue. In the present analysis, we considered each ROI from each patient as a separate piece of data, since each ROI in deep white matter could have a different blood supply and different ischemic damage.

Since the FWHM of PET data acquisition is known to be 6 mm (15), analysis of nominally smaller ROIs of less than 3 FWHM is meaningless. We could have selected smaller ROIs on the MTR maps, but these would have been less useful for correlation with the PET and MTR data. Thus, in this study, we used ROIs with a 21-mm diameter, based on the requirement of PET data analysis. A small region of CSF contamination might have been included in some cases, but we believe this effect was limited and that selected ROIs were located primarily in white matter.

The areas classified as group 0 (MTR $>$ 47.22%) showed normal signal intensity on T2-weighted images. Regional CBF values ranged from normal to slightly decreased, and $rCMRO_2$ values were normal. Therefore, the metabolic profile described by PET data was normal in this group.

The areas classified as group 1 (MTR values between 45.77% and 47.22%) were characterized by decreased rCBF, normal $rCMRO_2$, and increased rOEF-AI. In this group, the oxygen demand of brain tissue was partly compensated; and the brain tissue was thought to be viable and reversible, since the $rCMRO_2$ measured by PET was maintained within the normal range (25, 30, 32). We think that this result has important implications, because the areas showing a slightly decreased MTR may be

considered to be in a compromised vasculometabolic state and to remain reversible. Perfusion therapy, such as extra- or intracranial bypass surgery, is apparently indicated for patients who have lesions falling within this group.

Although the exact mechanism of the slight reduction of MTR in group 1 was not fully explained, a subtle constitutional change might occur in cell membranes, and thus the interaction between free water protons and macromolecules may be lowered. The major source of the MT phenomenon in white matter is thought to be myelin sheets of oligodendroglia with embedded protein (33). We could postulate that MTR values from white matter primarily reflect glial viability, since the major cellular component of white matter is glial cells. On the other hand, $rCMRO_2$ mostly reflects the metabolic activity of both neurons and glia. However, the activity of neurons is known to be greater than that of glia (34), and therefore we could consider $rCMRO_2$ as the neuronal viability. Hence, the slightly decreased MTRs and normal $rCMRO_2$ in group 1 might correspond to the subtle glial damage and intact neuronal tissue due to the mild ischemic insult. If the damage means a constitutional change of myelin, in which the interactions between free water and macromolecules are less frequent than those in normal tissue, this state may be potentially reversible. Although we cannot deny the possibility that the change involves subtle but irreversible microscopic changes, the former state is more reasonable for group 1, since the oligodendrocyte supports oxygen and metabolic supply to the neuronal cells (34) and this glial function was still retained in this group according to the result of $rCMRO_2$. Some studies have suggested the occurrence of a constitutional change in myelin and of the intactness of neuronal tissue in a chronic ischemic state (11–13, 24, 35).

The areas classified as group 2 (MTR $<$ 45.77%) were characterized by quantitatively decreased rCBF and $rCMRO_2$. The state of the brain tissue in this area was considered irreversible, because the decreased values of $rCMRO_2$ were demonstrated absolutely by PET (25, 30, 32). The signal intensity on normalized T2-weighted images in this area was increased, which meant that a normal constitution had not already existed. An irreversible loss of neurons and oligodendrocytes, demyelination, and reactive gliosis were postulated in this area (36–38). Finally, by using the MTR technique, we were able to classify ischemic areas into three groups: normal, reversible, and irreversible.

The increased rOEF on the lesional side was not detected with absolute values in a portion of group 1, but we were able to demonstrate this using the AI technique. Powers et al (18) reported that the wide range of normal values for absolute measurements with PET makes detection of abnormalities difficult. Variations of rOEF with absolute values were found to be greater than those of other parameters (39). The use of the AI technique has the advantage of improving sensitivity in identifying localized disease (18). Therefore, we think it is possible to isolate localized abnormalities with the AI technique. The AI technique, however, allows the ROI value to be classified only as abnormal and permits no conclusion about the opposite ROI value. So, it is worth analyzing not only absolute values but also those of AI. These combined techniques allow the possibility of demonstrating latent abnormalities.

A comparison between MTR and $rCMRO_2$ values is noteworthy. We found that the correlation between the reduction of MTR-AI and that of $rCMRO_2$-AI was statistically significant in long-standing ischemic brain tissue. Powers and coworkers (40, 41) found that the $rCMRO_2$ value is a good indicator of brain tissue viability, indicating that the MT phenomenon has a close relation to the viability of ischemic brain tissue and that the reduction of MTR could serve as a substitute marker of brain tissue viability measured by PET.

Conclusion

Compared with MTR values on the contralateral side, those on the lesional side revealed only a slight reduction in ischemic brain tissue. The areas classified as group 1 (MTR between 45.77% and 47.22%) were characterized by a maintained $rCMRO_2$ and increased rOEF-AI, which may be considered as viable tissue in a PET study. On the other hand, the areas in group 2 (MTR $<$ 45.77%) had absolutely decreased values of $rCMRO_2$, which may be considered irreversibly damaged. The correlation between the reduction of MTR and that of $rCMRO_2$ was statistically significant. MTR measurements in chronic cerebrovascular disease are useful for detecting hemodynamic abnormalities in PET.

References

1. Wolff SD, Balaban RS. **Magnetization transfer contrast (MTC) and tissue water proton relaxation in vivo.** *Magn Reson Med* 1989;10:135–144
2. Balaban RS, Ceckler TL. **Magnetization transfer contrast in magnetic resonance imaging.** *Magn Reson Q* 1992;8:116–137
3. Eng J, Ceckler TL, Balaban RS. **Quantitative 1H magnetization transfer imaging in vivo.** *Magn Reson Med* 1991;17:304–314
4. McGowan JC III, Schnall MD, Leigh JS. **Magnetization transfer imaging with pulsed off-resonance saturation: variation in contrast with saturation duty cycle.** *J Magn Reson Imaging* 1994;4:79–82
5. Gillams AR, Silver MS, Carter AP. **Clinical utility of a new contrast option from magnetization transfer contrast.** *J Magn Reson Imaging* 1995;5:545–550
6. Fralix TA, Ceckler TL, Wolff SD, Simon SA, Balaban RS. **Lipid bilayer and water proton magnetization transfer: effect of cholesterol.** *Magn Reson Med* 1991;18:214–223
7. Dousset V, Grossman RI, Ramer KN, et al. **Experimental allergic encephalomyelitis and multiple sclerosis: lesion characterization with magnetization transfer imaging.** *Radiology* 1992;182:483–491
8. Loevner LA, Grossman RI, Cohen JA, et al. **Microscopic disease in normal-appearing white matter on conventional MR images in patients with multiple sclerosis: assessment with magnetization transfer measurements.** *Radiology* 1995;196:511–515

9. Lexa FJ, Grossman RI, Rosenquist AC. **MR of wallerian degeneration in the feline visual system: characterization by magnetization transfer rate with histopathologic correlation.** *AJNR Am J Neuroradiol* 1994;15:201–212
10. Kimura H, Meaney DF, Mc Gowan JC, et al. **Magnetization transfer imaging of diffuse axonal injury following experimental brain injury in the pig: characterization by magnetization transfer ratio with histopathologic correlation.** *J Comput Assist Tomogr* 1996;20:540–546
11. Kurumatani T, Kudo T, Ikura Y, et al. **White matter changes in the gerbil brain under chronic cerebral hypoperfusion.** *Stroke* 1998;29:1058–1062
12. Kudo T, Takeda M, Tanimukai S, et al. **Neuropathologic changes in the gerbil brain after chronic hypoperfusion.** *Stroke* 1993; 24:259–264
13. Scremin OU, Jenden DJ. **Focal ischemia enhances choline output and decreases acetylcholine output from rat cerebral cortex.** *Stroke* 1989;20:92–95
14. Jope RS, Jenden DJ. **Choline and phospholipid metabolism and the synthesis of acetylcholine in rat brain.** *J Neurosci Res* 1979; 4:69–82
15. De Grado TR, Turkington TG, Williams JJ, Stearns CW, Hoffman JM, Coleman RE. **Performance characteristics of a whole-body PET scanner.** *J Nucl Med* 1994;35:1398–1406
16. Lammertsma AA, Jones T. **Correction for the presence of intravascular oxygen-15 in the steady-state technique for measuring regional oxygen extraction ratio in the brain, 1: description of the method.** *J Cereb Blood Flow Metab* 1983;3: 416–424
17. Lammertsma AA, Jones T, Frackowiak RS, Lenzi GL. **A theoretical study of the steady-state model for measuring regional cerebral blood flow and oxygen utilization using oxygen-15.** *J Comput Assist Tomogr* 1981;5:544–550
18. Powers WJ, Press GA, Grubb RL Jr, et al. **The effect of hemodynamically significant carotid artery disease on the hemodynamic status of the cerebral circulation.** *Ann Intern Med* 1987;106:27–34
19. Miller BL. **A review of chemical issues in 1H NMR spectroscopy: N-acetyl-L-aspartate, creatine and choline.** *NMR Biomed* 1991;4:47–52
20. Davie CA, Hawkins CP, Barker GJ, et al. **Detection of myelin breakdown products by proton magnetic resonance spectroscopy.** *Lancet* 1993;341:630–631
21. Matthews PM, Francis G, Antel J, Arnold DL. **Proton magnetic resonance spectroscopy for metabolic characterization of plaques in multiple sclerosis.** *Neurology* 1991;41:1251–1256
22. Miller DH, Austin SJ, Connelly A, Youl BD, Gadian DG, Mc Donald WI. **Proton magnetic resonance spectroscopy of an acute and chronic lesion in multiple sclerosis.** *Lancet* 1991;337: 58–59
23. Kruse B, Barker PB, van Zijl PC, Duyn JH, Moonen CT, Moser HW. **Multislice proton magnetic resonance spectroscopic imaging in X-linked adrenoleukodystrophy.** *Ann Neurol* 1994;36: 595–608
24. Handa Y, Kaneko M, Matuda T, Kobayashi H, Kubota T. **In vivo proton magnetic resonance spectroscopy for metabolic changes in brain during chronic cerebral vasospasm in primates.** *Neurosurgery* 1997;40:773–780
25. Mc Pherson RW, Koehler RC, Traystman RJ. **Effect of jugular venous pressure on cerebral autoregulation in dogs.** *Am J Physiol* 1988;255:H1516–H1524
26. Miller JD, Stanek AE, Langfitt TW. **A comparison of autoregulation to changes in intracranial and arterial pressure in the same preparation.** *Eur Neurol* 1971–72;6:34–38
27. Grubb RL Jr, Raichle ME, Phelps ME, Ratcheson RA. **Effects of increased intracranial pressure on cerebral blood volume, blood flow, and oxygen utilization in monkeys.** *J Neurosurg* 1975;43:385–398
28. Sadoshima S, Thames M, Heistad D. **Cerebral blood flow during elevation of intracranial pressure: role of sympathetic nerves.** *Am J Physiol* 1981;241:H78–H84
29. Rapela CE, Green HD, Denison AB Jr. **Baroreceptor reflexes and autorregulation of cerebral blood flow in the dog.** *Circ Res* 1967;21:559–5680
30. Kanno I, Uemura K, Higano S, et al. **Oxygen extraction fraction at maximally vasodilated tissue in the ischemic brain estimated from the regional CO2 responsiveness measured by positron emission tomography.** *J Cereb Blood Flow Metab* 1988;8: 227–235
31. Hoffman EJ, Huang SC, Phelps ME. **Quantitation in positron emission computed tomography, 1: effect of object size.** *J Comput Assist Tomogr* 1979;3:299–308
32. Carpenter DA, Grubb RL Jr, Tempel LW, Powers WJ. **Cerebral oxygen metabolism after aneurysmal subarachnoid hemorrhage.** *J Cereb Blood Flow Metab* 1991;11:837–844
33. Angevine JB. **The nervous tissue.** In: Fawcett DW, Raviola E, eds. Bloom and Fawcett: *A Textbook of Histology.* 12th ed. New York: Chapman & Hall; 1994:309–364
34. Edvinsson L, Mackenzie ET, Mc Culloch J. ***Cerebral Blood Flow and Metabolism.*** New York: Raven; 1993:142–152
35. Tsuchida C, Kimura H, Sadato N, Tsuchida T, Tokuriki Y, Yonekura Y. **Evaluation of brain metabolism in steno-occlusive carotid artery disease by proton MR spectroscopy: a correlative study with oxygen metabolism by PET.** *J Nucl Med* 2000;41: 1357–1362
36. Ohta H, Nishikawa H, Kimura H, Anayama H, Miyamoto M. **Chronic cerebral hypoperfusion by permanent internal carotid ligation produces learning impairment without brain damage in rats.** *Neuroscience* 1997;79:1039–1050
37. Dubas F, Gray F, Roullet E, Escourolle R. **Arteriopathic leukoencephalopathy (17 anatomo-clinical cases).** *Rev Neurol (Paris)* 1985;141:93–108
38. Sekhon LH, Spence I, Morgan MK, Weber NC. **Chronic cerebral hypoperfusion: pathological and behavioral consequences.** *Neurosurgery* 1997;40:548–556
39. Yamaguchi T, Kanno I, Uemura K, et al. **Reduction in regional cerebral metabolic rate of oxygen during human aging.** *Stroke* 1986;17:1220–1228
40. Powers WJ, Grubb RL Jr, Raichle ME. **Physiological responses to focal cerebral ischemia in humans.** *Ann Neurol* 1984;16: 546–552
41. Powers WJ, Grubb RL Jr, Darriet D, Raichle ME. **Cerebral blood flow and cerebral metabolic rate of oxygen requirements for cerebral function and viability in humans.** *J Cereb Blood Flow Metab* 1985;5:600–608